Journal of Geosciences and Geomatics, 2017, Vol. 5, No. 2, 65-77
Available online at http://pubs.sciepub.com/jgg/5/2/3

DOI:10.12691/jgg-5-2-3

Transitional Basalts and Eruptive Dynamisms around Nkoumelap Locality (West of the Bamoun Plateau, Cameroon Volcanic Line): Petrography and Volcanic Risks' Evaluation

Luc Achille ZIEM A BIDIAS[1,2,*], Amidou MOUNDI[1], Jonas Didero TAKODJOU WAMBO[1]

[1]Département des Sciences de la Terre et de l'Univers, Faculté des Sciences, Université de Yaoundé 1, BP 812, Yaoundé, Cameroun
[2]Laboratoire de Géologie, École Normale Supérieure, Université de Yaoundé-1, BP 047, Yaoundé, Cameroun
*Corresponding author: bzila2001@yahoo.fr.

Received January 27, 2017; Revised March 15, 2017; Accepted April 07, 2017

Abstract Diverse eruptive dynamisms have occurred in the west side of the Bamoun plateau, producing ashes, scoria, lapilli, blocks and bombs. The lavas are essentially transitional basalts, and rhyolites. Transitional basalts are rather exceptional in the Cameroon Volcanic Line (CVL). The chemical composition of the minerals of these basalts is indicative of the thermobarometric conditions of their formation. In the locality of Nkoumelap situated to the West of the Bamoun plateau, they crystallized at low pressure (1.8 Kb) and relatively high temperatures (from 1110°C to 862°C in clinopyroxenes and 1044°C to 801°C in opaque minerals of transitional basalts) and differ significantly from the alkali basalts of the same plateau as well as from all the typical alkali basalts of the CVL. Measures of the distribution of volcanic products coupled to the volcanic history of the region could enhance understanding of the intensity of volcanic events and facilitate evaluation of induced risks. The Landstat 7 ETM$^+$ data of the region was used to elaborate a hazards map of the zone, highlighting volcanic risks. This study, realized in the Bamoun plateau, is the baseline for a vast cartography program of the hazards and risks along the CVL. It could help to better protect the population and efficiently manage risks in case the volcanic activity is revived.

Keywords: *eruptive dynamisms, transitional basalts, hazards, risks, Cameroon Volcanic Line*

Cite This Article: Luc Achille ZIEM A BIDIAS, Amidou MOUNDI, and Jonas Didero TAKODJOU WAMBO, "Transitional Basalts and Eruptive Dynamisms around Nkoumelap Locality (West of the Bamoun Plateau, Cameroon Volcanic Line): Petrography and Volcanic Risks' Evaluation." *Journal of Geosciences and Geomatics*, vol. 5, no. 2 (2017): 65-77. doi: 10.12691/jgg-5-2-3.

1. Introduction

Many works have been carried out with the aims to better understand the volcanism of the Bamoun Plateau in Cameroon Volcanic Line. The most recent are those of [1,2,3]. According to these authors, there are transitional basalts, alkaline basalts and ankaramites associated with some felsic lavas. Nevertheless, in the west side of this plateau, precisely in the region of Nkoumelap and its surroundings, there are no consistent petrographic data, and no studies on the risks arising from volcanic activity have yet been carried out.

The Bamoun plateau belongs to the Cameroon volcanic line (CVL) (Figure 1). The various lavas and varied volcanic products show that several types of eruptive dynamism have manifested themselves. Detailed analysis of Landsat-7 ETM$^+$ and the volcanic and petrographic data can contribute to the identification of different types of hazards and risks related to the volcanic activity.

The aim of this paper is to present some petrographic and mineralogical characteristics of the basalts of the Nkoumelap sector, as well as the eruptive dynamisms in the West of the Bamoun plateau and the associated risks. Since volcanism in this sector stands as a major risk, it is important to evaluate the volcanic threats and to endeavour to mitigate their consequences on human beings and infrastructure.

2. Localisation and Geological Setting

The study area is located between latitudes 5°38' and 5°55' North and longitudes 10°42' and 10°48' East. The relief is a plateau, made of hills with gentle slopes dominated by three volcanic cones at Nka'nyam (1445 m of asl), Nkoumelap (1485 m of asl) and Bangourain (1585 m of asl). The mafic lavas are Eocene fissural basalts [4] overlying the Pan-African basement (Figure 2). These lavas have been identified as basalts without olivine with a transitional character and are among the oldest basalts on the CVL aged of 51.8 ± 1.2 Millions of years [1]. The identification of the tectonic structures (lineaments)

associated with the volcanoes of the region could be made. Observing the Landsat images allows us to note nearly 200 lineaments of various orientations (Figure 3), despite soil and volcanic cover. There are also some circular and polygonal structures materializing domes and cones. The rosace of the lineamentary directions (Figure 3) representing the regional range of the fracturing, show that the average fracture of the substratum is oriented W - E. Several directions are also observed in the crystalline substratum: (1) a major direction N50-60; (2) four minor directions N40, N70-90, N120-130 and N170. The cones of the volcanic buildings are aligned in various directions (N20-30, N70-80, and N-S). These observations make it possible to infer that there should be a close relationship between volcanism and tectonics through open faults in the ante-volcanic substratum which would probably have served as a passageway for the various lavas.

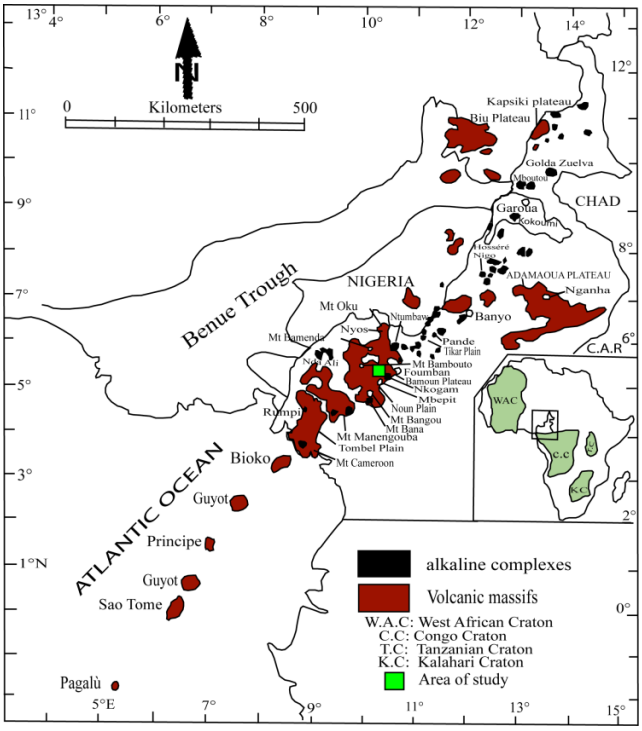

Figure 1. Location of the study area (green square) along the Cameroon Volcanic Line (adapted after [6]). Location of seamounts after [7]. Insert bottom right is after [8]

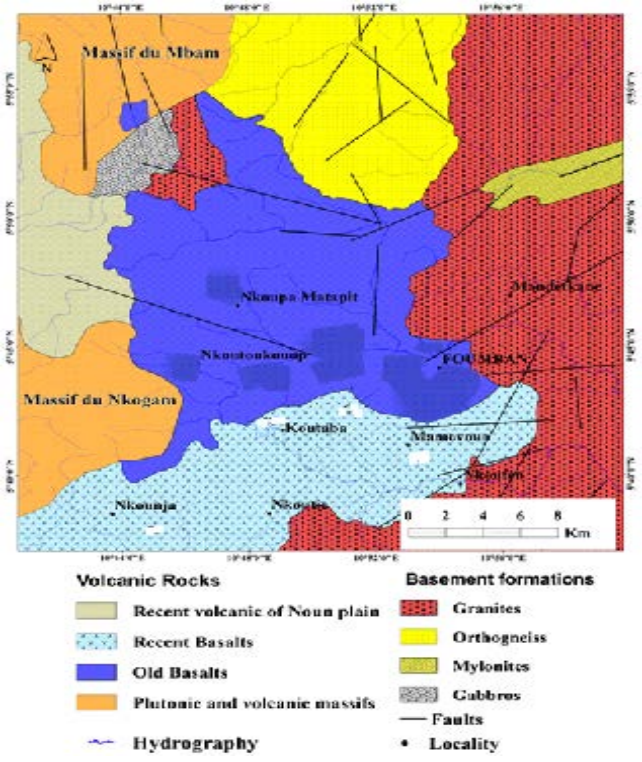

Figure 2. Simplified geological map of the Bamoun area (after [3])

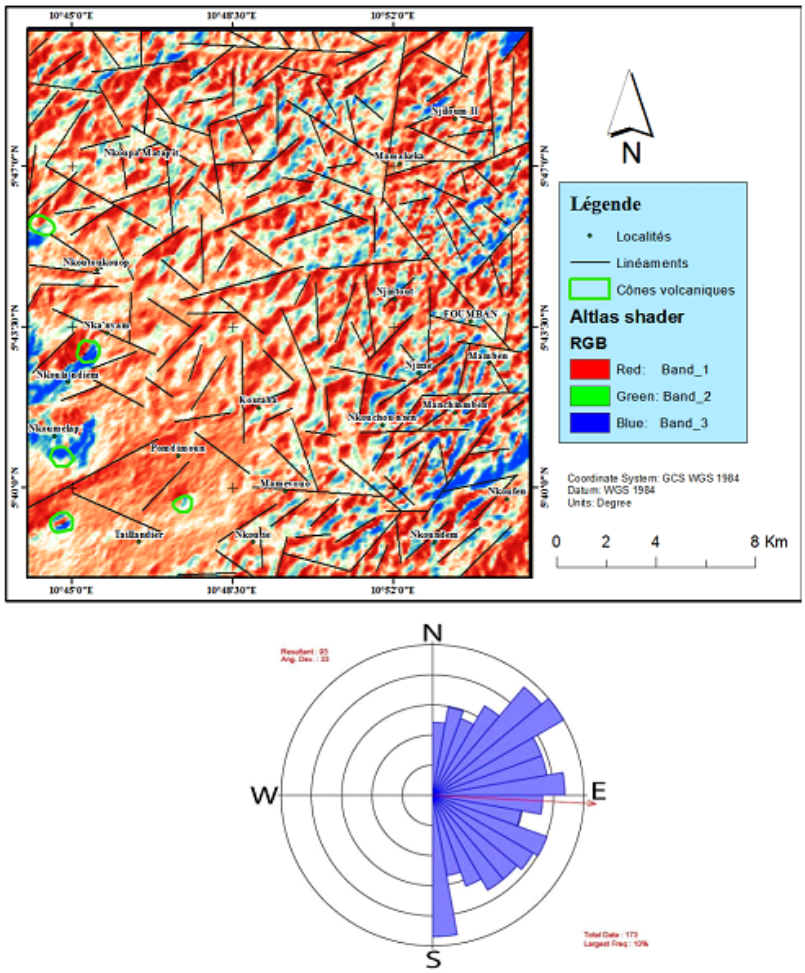

Figure 3. Volcano-tectonic map and rosace of the lineamentary directions (below) of the sector Koutaba - Nkoumelap. The red arrow represents the mean lineamentary direction

Table 1. Representative microprobe analyses of clinopyroxenes, plagioclases, magnetites and ilmenites. ph: phenocryst; mph: microphenocryst; m: microlite; c: core; r: rim; gm: groundmass. Working conditions: 15 KeV; 10-12 nA.

Clinopyroxenes samples	ZB7	ZB7	ZB7	ZB7	ZB2	ZB2	ZB2	ZB2	ZB2
	mph	gm	mph	gm	gm	gm	gm	mph	mph
SiO2	50,55	50,47	50,92	50,40	50,18	50,56	50,81	51,48	51,11
TiO2	1,28	1,47	1,35	1,41	1,35	1,32	1,28	0,79	1,00
Al2O3	2,30	2,16	1,50	2,27	2,03	2,15	2,14	1,33	1,37
Cr2O3	0,03	0,02	0,01	0,05	0,01	0,03	0,00	0,00	0,00
Fe2O3 calc.	1,87	3,20	2,28	2,42	1,76	2,79	2,59	0,70	2,47
FeO calc.	8,97	8,66	10,14	8,07	12,56	9,95	10,23	16,10	10,53
MnO	0,20	0,24	0,25	0,20	0,30	0,26	0,31	0,42	0,30
MgO	14,77	14,87	15,85	14,57	13,42	14,04	14,19	14,21	14,63
CaO	19,30	19,36	17,32	20,18	18,07	19,40	19,46	15,13	18,63
Na2O	0,29	0,31	0,27	0,31	0,28	0,32	0,25	0,21	0,26
K2O	0,00	0,01	0,00	0,01	0,00	0,01	0,00	0,01	0,00
Total (Wt.%)	**99,57**	**100,77**	**99,88**	**99,88**	**99,95**	**100,82**	**101,25**	**100,37**	**100,31**
Si	1,897	1,878	1,907	1,887	1,901	1,888	1,890	1,946	1,916
Al iv	0,102	0,095	0,066	0,100	0,091	0,094	0,094	0,054	0,060
Al vi	0,000	0,000	0,000	0,000	0,000	0,000	0,000	0,005	0,000
Ti	0,036	0,041	0,038	0,040	0,039	0,037	0,036	0,022	0,028
Cr	0,001	0,001	0,000	0,002	0,000	0,001	0,000	0,000	0,000
Fe3+	0,053	0,090	0,064	0,068	0,050	0,078	0,073	0,020	0,070
Fe2+	0,282	0,270	0,317	0,253	0,398	0,311	0,318	0,509	0,330
Mn	0,006	0,007	0,008	0,006	0,009	0,008	0,010	0,013	0,010
Mg	0,826	0,825	0,885	0,813	0,758	0,782	0,787	0,801	0,818
Ca	0,776	0,772	0,695	0,809	0,734	0,776	0,775	0,693	0,749
Na	0,021	0,023	0,020	0,022	0,020	0,024	0,018	0,015	0,019
K	0,000	0,000	0,000	0,000	0,000	0,000	0,000	0,001	0,000
Total	**4,000**	**4,000**	**4,000**	**4,000**	**4,000**	**4,000**	**4,000**	**4,000**	**4,000**
Wo(Ca)	39,92	39,31	35,29	41,51	37,64	39,7	39,51	31,33	37,89
En (Mg)	42,53	42,01	44,93	41,72	38,88	39,98	40,09	40,94	41,4
Fs(Fe2+Fe3+Mn)	17,54	18,68	19,79	16,77	23,48	20,32	20,4	27,72	20,71

Clinopyroxenes samples	**ZB55**	**ZB55**	**ZB55**	**ZB59**	**ZB59**	**ZB59**	**ZB59**	**ZB59**	**ZB59**	**ZB59**
	gm	mph	gm	gm	mph	mph	gm	mph	m	m
SiO2	49,19	49,37	46,92	51,45	51,08	50,19	51,83	51,87	49,72	50,98
TiO2	1,65	1,25	4,05	0,89	0,81	1,13	0,96	1,06	1,41	1,06
Al2O3	2,72	4,24	3,31	1,44	1,80	2,42	1,54	2,25	2,06	2,03
Cr2O3	0,01	0,00	0,00	0,00	0,00	0,00	0,00	0,00	0,00	0,00
Fe2O3 calc.	2,69	2,38	1,43	2,27	2,63	4,15	2,09	1,82	3,06	3,14
FeO calc.	12,08	12,89	14,45	11,22	11,26	7,86	10,47	8,29	11,91	8,13
MnO	0,39	0,39	0,38	0,38	0,39	0,34	0,35	0,27	0,35	0,24
MgO	13,51	12,11	12,35	14,65	14,97	14,43	14,97	15,31	13,24	15,48
CaO	17,21	15,50	16,12	18,33	17,46	19,87	18,85	20,02	18,35	19,19
Na2O	0,34	0,70	0,45	0,24	0,24	0,35	0,24	0,32	0,29	0,29
K2O	0,04	0,72	0,05	0,00	0,00	0,00	0,02	0,00	0,01	0,01
Total (Wt.%)	**99,82**	**99,55**	**99,50**	**100,88**	**100,64**	**100,76**	**101,33**	**101,19**	**100,40**	**100,55**
Si	1,867	1,878	1,805	1,920	1,909	1,870	1,919	1,908	1,881	1,893
Al iv	0,122	0,122	0,150	0,063	0,079	0,106	0,067	0,092	0,092	0,089
Al vi	0,000	0,069	0,000	0,000	0,000	0,000	0,000	0,006	0,000	0,000
Ti	0,047	0,036	0,117	0,025	0,023	0,032	0,027	0,029	0,040	0,030
Cr	0,000	0,000	0,000	0,000	0,000	0,000	0,000	0,000	0,000	0,000
Fe3+	0,077	0,068	0,041	0,064	0,074	0,116	0,058	0,050	0,087	0,088
Fe2+	0,384	0,410	0,465	0,350	0,352	0,245	0,324	0,255	0,377	0,252
Mn	0,013	0,012	0,012	0,012	0,012	0,011	0,011	0,009	0,011	0,007
Mg	0,764	0,687	0,708	0,815	0,834	0,802	0,826	0,839	0,747	0,857
Ca	0,700	0,632	0,665	0,733	0,699	0,793	0,748	0,789	0,744	0,763
Na	0,025	0,051	0,034	0,017	0,017	0,026	0,017	0,023	0,021	0,021
K	0,002	0,035	0,002	0,000	0,000	0,000	0,001	0,000	0,000	0,000
Total	**4,000**	**4,000**	**4,000**	**4,000**	**4,000**	**4,000**	**4,000**	**4,000**	**4,000**	**4,000**
Wo(Ca)	36,12	34,92	35,14	37,12	35,46	40,33	38,01	40,63	37,83	38,79
En (Mg)	39,46	37,96	37,43	41,3	42,31	40,76	41,99	43,22	37,99	43,54
Fs(Fe2+Fe3+Mn)	24,42	27,12	27,42	21,58	22,23	18,91	20	16,15	24,17	17,66
Plagioclases samples	**ZB7**	**ZB7**	**ZB7**	**ZB2**	**ZB2**	**ZB2**	**ZB2**	**ZB2**	**ZB2**	
	m	m	m	ph,c	ph, r	ph, r	ph,c	ph, c	ph, r	
SiO2	52,06	54,04	52,18	56,90	56,19	54,79	55,84	54,74	54,39	
TiO2	0,09	0,21	0,16	0,17	0,06	0,15	0,12	0,09	0,12	
Al2O3	29,59	27,72	29,29	27,09	27,20	27,77	26,92	27,60	27,58	
Fe2O3	0,67	1,14	0,66	0,45	0,50	0,89	0,60	0,36	0,78	
MnO	0,03	0,00	0,02	0,01	0,00	0,01	0,03	0,04	0,04	
MgO	0,10	0,08	0,08	0,05	0,05	0,12	0,07	0,08	0,10	
CaO	13,42	11,28	12,90	10,03	10,17	11,12	10,30	10,56	11,21	
SrO	0,00	0,00	0,00	0,00	0,00	0,00	0,00	0,00	0,00	
BaO	0,00	0,00	0,00	0,00	0,00	0,00	0,00	0,00	0,00	
Na2O	3,94	4,89	4,36	5,54	5,53	5,12	5,54	5,26	4,93	
K2O	0,22	0,37	0,27	0,69	0,64	0,50	0,65	0,51	0,49	
Rb2O	0,00	0,00	0,00	0,00	0,00	0,00	0,00	0,00	0,00	
Total	**100,11**	**99,73**	**99,89**	**100,94**	**100,33**	**100,47**	**100,07**	**99,24**	**99,63**	
Si	2,369	2,458	2,379	2,542	2,528	2,473	2,523	2,492	2,474	
Ti	0,003	0,007	0,005	0,006	0,002	0,005	0,004	0,003	0,004	
Al	1,587	1,486	1,574	1,426	1,442	1,477	1,433	1,481	1,479	
Fe3+	0,023	0,039	0,023	0,015	0,017	0,030	0,020	0,012	0,027	
Mn	0,001	0,000	0,001	0,001	0,000	0,000	0,001	0,001	0,002	
Mg	0,007	0,006	0,005	0,004	0,003	0,008	0,005	0,006	0,006	
Ca	0,654	0,550	0,630	0,480	0,490	0,538	0,499	0,515	0,547	
Ba	0,000	0,000	0,000	0,000	0,000	0,000	0,000	0,000	0,000	
Na	0,347	0,431	0,385	0,480	0,482	0,448	0,485	0,464	0,435	
K	0,013	0,021	0,016	0,039	0,036	0,029	0,037	0,029	0,028	
Rb	0,000	0,000	0,000	0,000	0,000	0,000	0,000	0,000	0,000	
Total	**5,003**	**4,998**	**5,018**	**4,992**	**5,000**	**5,007**	**5,008**	**5,005**	**5,001**	
Ab	**34,25**	**43,02**	**37,35**	**48,03**	**47,79**	**44,17**	**47,52**	**45,99**	**43,07**	
An	**64,49**	**54,84**	**61,10**	**48,03**	**48,59**	**53,01**	**48,82**	**51,09**	**54,15**	
Or	**1,27**	**2,14**	**1,55**	**3,95**	**3,62**	**2,82**	**3,66**	**2,92**	**2,79**	

Plagioclases samples	**ZB55**	**ZB55**	**ZB55**	**ZB55**	**ZB59**	**ZB59**	**ZB59**	**ZB59**	**ZB59**	**ZB59**
	ph, r	ph, c	ph, r	ph, r	ph, c	ph, r	m	ph, c	ph, r	m
SiO2	56,26	57,69	55,67	56,06	55,84	55,87	52,82	55,89	54,35	53,19
TiO2	0,82	0,16	0,23	0,17	0,09	0,09	0,06	0,13	0,13	0,10
Al2O3	25,43	25,63	24,83	26,28	26,99	27,15	28,86	27,27	27,85	28,80
Fe2O3	3,01	1,26	2,86	1,51	0,59	0,93	0,75	0,79	0,89	0,78
MnO	0,05	0,01	0,04	0,02	0,00	0,03	0,00	0,00	0,00	0,00
MgO	0,01	0,03	0,83	0,12	0,06	0,08	0,11	0,07	0,13	0,10
CaO	8,12	7,79	9,00	8,60	10,11	10,02	12,34	10,12	11,55	12,47
SrO	0,00	0,00	0,00	0,00	0,00	0,00	0,00	0,00	0,00	0,00
BaO	0,23	0,15	0,08	0,10	0,00	0,00	0,00	0,00	0,00	0,00
Na2O	6,24	6,47	5,99	6,33	5,71	5,69	4,48	5,71	5,10	4,44
K2O	0,94	1,01	0,60	0,62	0,44	0,52	0,30	0,50	0,44	0,30
Rb2O	0,00	0,00	0,00	0,00	0,00	0,00	0,00	0,00	0,00	0,00
Total	**101,11**	**100,20**	**100,13**	**99,80**	**99,84**	**100,38**	**99,73**	**100,49**	**100,44**	**100,18**
Si	2,534	2,597	2,531	2,541	2,525	2,516	2,407	2,514	2,458	2,413
Ti	0,028	0,005	0,008	0,006	0,003	0,003	0,002	0,004	0,004	0,003
Al	1,350	1,360	1,331	1,404	1,438	1,441	1,550	1,445	1,484	1,540
Fe3+	0,102	0,043	0,098	0,052	0,020	0,032	0,026	0,027	0,030	0,027
Mn	0,002	0,000	0,002	0,001	0,000	0,001	0,000	0,000	0,000	0,000
Mg	0,001	0,002	0,057	0,008	0,004	0,005	0,007	0,005	0,009	0,007
Ca	0,392	0,376	0,438	0,418	0,490	0,484	0,603	0,488	0,560	0,606
Ba	0,004	0,003	0,001	0,002	0,000	0,000	0,000	0,000	0,000	0,000
Na	0,545	0,565	0,528	0,556	0,500	0,497	0,396	0,498	0,448	0,390
K	0,054	0,058	0,035	0,036	0,025	0,030	0,017	0,029	0,025	0,017
Rb	0,000	0,000	0,000	0,000	0,000	0,000	0,000	0,000	0,000	0,000
Total	**5,011**	**5,008**	**5,028**	**5,021**	**5,006**	**5,008**	**5,009**	**5,009**	**5,017**	**5,004**
Ab	**55,00**	**56,56**	**52,74**	**55,09**	**49,26**	**49,17**	**38,99**	**49,10**	**43,34**	**38,52**
An	**39,55**	**37,61**	**43,78**	**41,37**	**48,24**	**47,85**	**59,31**	**48,09**	**54,21**	**59,78**
Or	**5,45**	**5,82**	**3,48**	**3,54**	**2,50**	**2,98**	**1,70**	**2,81**	**2,45**	**1,69**

Magnetite samples	**ZB7**	**ZB2**	**ZB2**
SiO2	0,242	0,616	0,234
Al2O3	1,389	1,778	1,947
TiO2	20,98	20,12	21,21
Fe2O3	22,95	25,08	24,13
FeO	47,09	49,18	49,91
MnO	2,322	0,685	0,832
MgO	0,036	0,146	0,063
CaO	0,104	0,018	0,039
Cr2O3	0,082	0,051	0,06
V2O3	0	0	0
NiO	0	0	0,02
ZnO	0	0	0
Na20	0	0	0
K20	0,001	0,014	0,003
Total (Wt.%)	**95,19**	**97,69**	**98,45**
Si	0,01	0,023	0,009
Al	0,064	0,08	0,087
Ti	0,619	0,577	0,604
Fe+3	0,677	0,719	0,687
Fe+2	1,545	1,568	1,58
Mn	0,077	0,022	0,027
Mg	0,002	0,008	0,004
Ca	0,004	0,004	0,002
Cr	0,003	0,002	0,002
V	0	0	0
Ni	0	0	0
Zn	0	0	0
Na	0	0	0
K	0	0	0
Total	**3**	**3**	**3**
X'USP	0,645	0,624	0,647

Ilmenite sample	**ZB7**	**ZB7**	**ZB7**	**ZB2**	**ZB59**
SiO2	0,04	0,00	0,02	0,03	0,05
Al2O3	0,09	0,05	0,13	0,05	0,01
TiO2	48,59	48,43	48,40	50,57	49,55
FeOt	47,16	47,90	47,62	46,82	47,47
MnO	0,37	0,38	0,40	0,50	1,55
MgO	1,90	1,71	2,32	1,64	0,03
CaO	0,16	0,10	0,12	0,12	0,19
Cr2O3	0,00	0,00	0,01	0,01	0,00
V2O3	0,00	0,00	0,00	0,00	0,00
NiO	0,00	0,05	0,06	0,00	0,02
ZnO	0,00	0,00	0,00	0,00	0,00
Na20	0,00	0,00	0,01	0,01	0,00
K20	0,00	0,00	0,01	0,00	0,02
Total	98,32	98,61	99,93	99,75	98,90
%Fe2O3	**8,21**	**8,83**	**9,80**	**5,45**	**5,27**
%FeO	**39,77**	**39,95**	**38,80**	**41,91**	**42,73**
Total (Wt.%)	99,14	99,50	100,92	100,30	99,43
Structural formulae (base 2 cations)					
Si	0,0010	0,0000	0,0005	0,0007	0,0013
Al	0,0027	0,0015	0,0039	0,0015	0,0003
Ti	0,9073	0,9043	0,9037	0,9442	0,9252
Fe+2	0,8257	0,8296	0,8056	0,8703	0,8872
Fe+3	0,1535	0,1649	0,1832	0,1019	0,0985
Mn	0,0078	0,0079	0,0085	0,0106	0,0326
Mg	0,0704	0,0631	0,0858	0,0608	0,0012
Ca	0,0043	0,0026	0,0031	0,0031	0,0051
Cr	0,0000	0,0000	0,0002	0,0002	0,0000
V	0,0000	0,0000	0,0000	0,0000	0,0000
Ni	0,0000	0,0010	0,0012	0,0001	0,0004
Zn	0,0000	0,0000	0,0000	0,0000	0,0000
Na	0,0000	0,0000	0,0004	0,0003	0,0000
K	0,0000	0,0000	0,0003	0,0000	0,0007
Total	**1,9727**	**1,9750**	**1,9963**	**1,9937**	**1,9525**

3. Material and Methods

The representative microprobe analysis of various minerals of the selected samples (Table 1) were realised by microprobe CAMECA SX 100 in the "Domaines Océaniques du Département des Sciences de la Terre" laboratory of "Institut Universitaire Européen de la Mer" in the University of "Bretagne Occidentale, Service Microsonde Ouest" in Brest (France).

Mapping of the volcanic hazards was done using the following data: (1) the Landsat-7 ETM+ images of the study area, which corresponds to the zone 32 of the cartographic projection Universal Transverse Mercator (UTM) using the WGS 84 geodesic system of reference; (2) the SRTM and DEM satellite images; (3) geologic map (scale 1/500 000 square degrees) of Foumban [5] and (4) the topographic map (scale 1/200 000) covering the explored zone.

ArcGIS 10, ERDAS IMAGINE 2014, and Geomatica 2012 softwares were used for analysis of the maps. The pre-treatment operations of the images consisted of radiometric and geometric corrections. This was aimed at correcting the distortions caused by movements of the platform as well as image errors caused by atmospheric disturbances. The corrected images were further treated to increase their visual perception which enabled a better visualisation of the discontinuities and a better appreciation of the variations of the relief. The data was then subject to Principal Component Analysis (PCA) and spatial filtering.

(1) ***Principal Component Analysis (PCA).***

The PCA enables equivalent definitions depending on whether focus is on the individual representation (in this case, the pixel of the image), on the variable representation or on their simultaneous representations. In PCA the matrix of the data is supposed to be from the observation of random independent ***n*** vectors ($x_1,\ldots, x_n$). Then a system of representation of reduced scale is constructed which preserves the distances between the individuals. PCA can thus be seen as a compression with a controlled loss of information. To make a geometric representation, a distance between two points in space is selected. The distance used by the PCA in space where the units are represented, is the classical Euclidean distance. The distance between two units u_i and $u_{i'}$ is equal to:

$$d^2(u_i, u_{i'}) = \sum_{j=1}^{p} (X_{ij} - X_{i'j})^2.$$

With this distance, all the variables play the same role and the axes defined by the variables form the orthogonal basis. To this distance, a scalar product between two vectors is associated:

$$\left\langle \overrightarrow{ou_i}, \overrightarrow{ou_{i'}} \right\rangle = \sum_{j=1}^{p} X_{ij} X_{i'j} = {}^t U_i U_{i'}$$

As well as the magnitude of the vector:

$$\left\| \overrightarrow{ou_i} \right\|^2 = \sum_{j=1}^{p} X_{ij}{}^2 = {}^t U_i U_i.$$

CPA made it possible to avoid redundancies thereby improving on the contrast of the initial Landsat-7 ETM+ image of the study area. This technique also reduces the number of bands to be treated by compressing the information in an ordered manner [9]. The six canals ETM+ 1, 2, 3, 4, 5 and 7 are all at a resolution of 30 m and are consequently chosen for the PCA, except the ETM+ 6(1), 6(2) canals which have a resolution of 60 m and the panchromatic band which have a resolution of 15 m. The results of the first two components (PCA1 and PCA2), respectively 78.3 and 9.2% define the information contained in the original multispectral image of nine bands. The structural data from the field also helped to interpret and validate the geological structures and the relief shapes revealed by satellite images. The transformed images obtained in this manner and grouping of the maximum information, were then filtered.

(2) ***Spatial filtering***.

In this study the convolution applies on an image $I(x, y)$ with respect to $f(x, y)$ called impulse response (or convolution operator) of the filter. In the case of continuous data, the filtered image is given by:

$$I_f(x, y) = (f \times I)(x, y)$$
$$= \int_{-\infty}^{+\infty} \int_{-\infty}^{+\infty} f(x', y') I(x - x', y - y') dx' dy'.$$

In the case of discrete data and to take the simplified example of a square image, the domains of I and f have end points. The domain of I is $[-N/2, +N/2]^2$ if N represents the size of the image and the domain of f is $[-K/2, +K/2]^2$ with $K \leq N$. The convolution is written as:

$$I_f(x, y) = (f \times I)(x, y)$$
$$= \sum_{i'=-k/2}^{i'=+k/2} \sum_{j'=-k/2}^{j'=+k/2} f(i - i', j - j') I(i', j').$$

Sobel's directional filters were used. They are applied in four principal directions: N-S, E-W, NE-SW, SE-NW. The operator uses convolution matrix. These 3x3 matrix filters were applied to the new PCA canals to stress on the lithologic discontinuities, allowing qualification of the relief forms. The sum of these treatments on the Landsat image (new PCA canals transformed by directional filters) provided complementary visual support on which the photo-interpretation and zoning of hazards relied.

4. Results and Discussion

4.1. Petrography and Mineralogy of Transitional Basalts

The outcrops of the transitional basalts occur in blocks in the localities of Nka'nyam and Nkoutoukouop, or in the form of gigantic lava flow forming a wall in Nkoumelap. They have doleritic and microlitic textures, varying from aphyric to porphyric terms (Figure 4). The size and shape of the minerals and the texture of these basalts are indicative of many crystallization phases. The volcanic glass constitutes less than 5% of the whole rock. Transitional basalts are characterised by the absence of

modal olivine. They consist mainly of plagioclase, clinopyroxene, ilmenite, and magnetite.

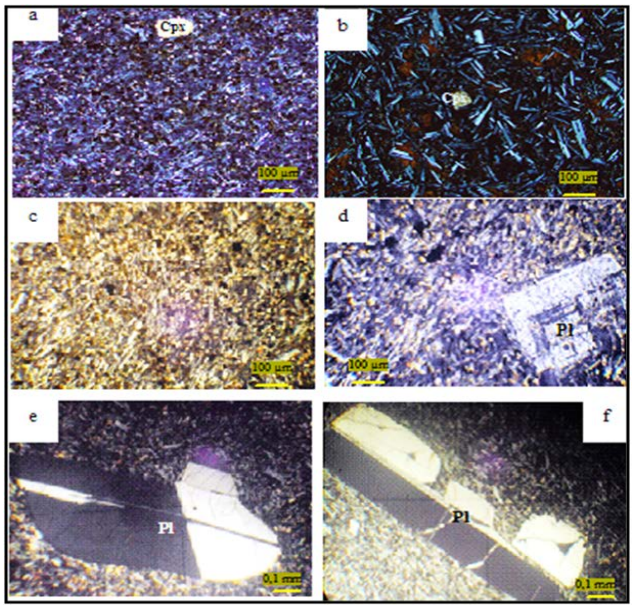

Figure 4. Representative photomicrographs (a,b,c,d) showing some textures and the mineralogical associations. Microlitic texture averagely porphyric (a, sample TA9) and doleritic (b, sample ZB5) in a basalt; aphyric texture (c, sample ZB7); zoned phenocrysts (d, ZB59) and twinning (e,f. ZB2) in transitional basalts with porphyric texture

Phenocrysts consist of plagioclases alone. They are found also as microlites associated to microcryst of clinopyroxenes and opaque minerals. They present several twins (Figure 4 e, f) and zonations (Figure 4d), and occupy about 75% of the basalt volume. Phenocrysts range from andesine ($An_{37,61-48,82}Ab_{47,52-56,56}Or_{3,66-5,82}$) to labrador ($An_{51,09-54,26}Ab_{43,34-45,99}Or_{2,45-2,92}$) whereas microlites are labrador ($An_{54,84-64,49}Ab_{34,25-43,02}Or_{1,27-2,14}$) (Table 1).

Clinopyroxenes are generally in the form of microcryst (Figure 4a, b) in some sub-automorphic sections (diameter ≤ 0.4 mm). They all correspond to the Quad (Figure 5a) and plot in the augite domain ($Ca_{31,3-41,5}$ $Mg_{37,4-44,9}$ $Fet+Mn_{16,1-27,7}$) in the Ca-Fe-Mg diagram (Figure 5c). According to the Ti/(Ca + Na) diagram of [10], the clinopyroxene belong to "tholeiitic and calc-alkali basalts" (Figure 5b). Ti and Al are lower in clinopyroxene as compared to those from olivine basalts of Bamoun area (Table 2).

This difference is of petrological significance since Ti and Al contents of clinopyroxenes are related to the crystallization condition and the initial magma composition [11,12,13]. They are crystallized in conditions of low pressure (Figure 5d).

The amounts of Ca + Na (0.7 to 0.8) in the clinopyroxenes are typical of transitional basalts according to [10]. All these characteristics are close to those of the clinopyroxenes of rocks of the East-African rifts and some oceanic islands, such as Kerguelen [14], the Fangataufa atoll [15,16] and Hawaii.

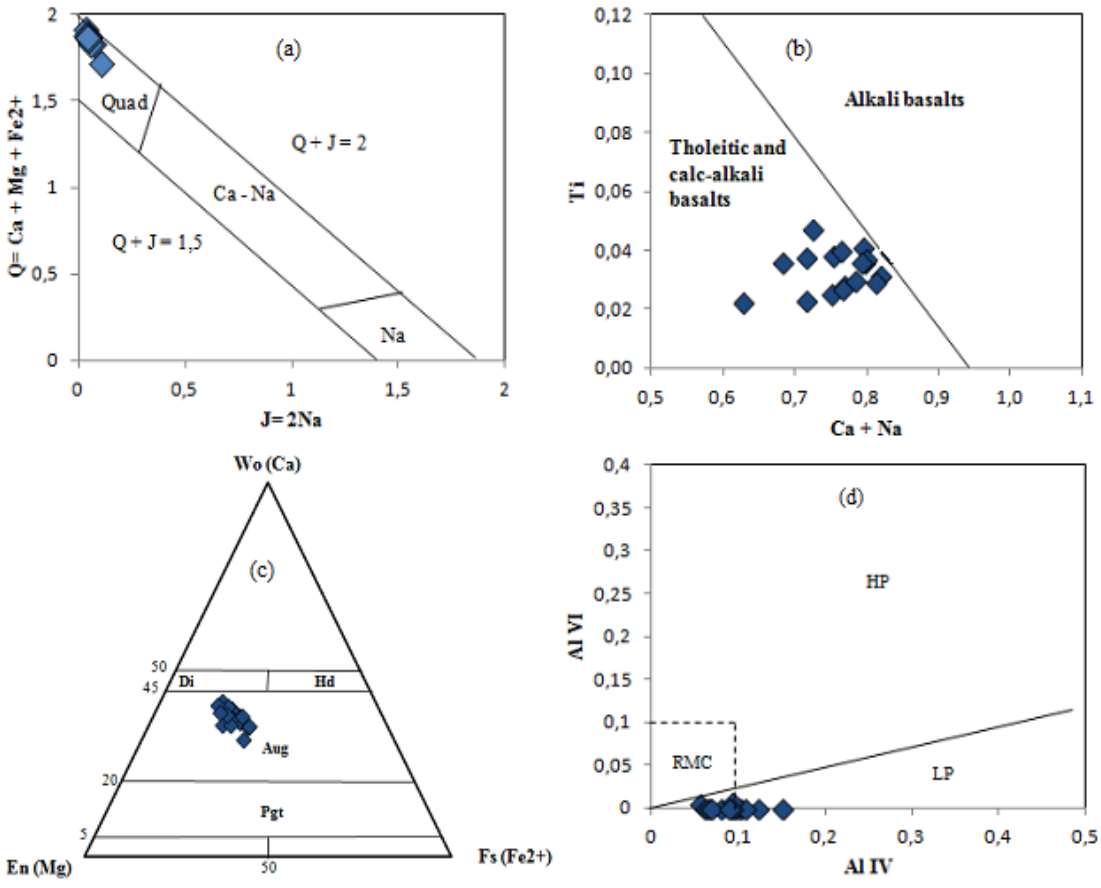

Figure 5. Chemical classification of pyroxenes in transitional basalts. (a) Position of pyroxenes in transitional basalt in the Q-J diagram of [22]; (b) Distribution of clinopyroxene of basalt in the Ti/(Ca + Na) diagram of [10]; (c) Mg-Ca-Fe^{2+}+Fe^{3+}+Mn diagram of pyroxenes [16]; (d) Position of clinopyroxenes in transitional basalts in the Al^{IV} vs. Al^{IV} diagram [23,24]. The domain limits are of [25]. RMC: fields of refractory mantle clinopyroxene [26]. HP=high pressure; LP=low pressure

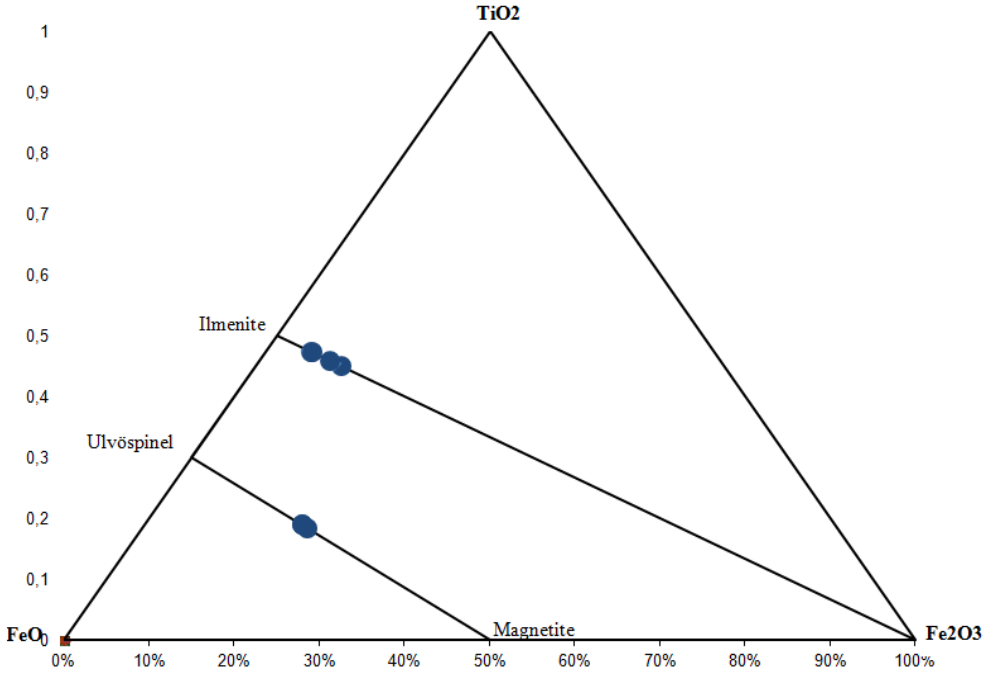

Figure 6. TiO_2 – FeO – Fe_2O_3 diagram giving the composition of the oxides of transitional basalts

Table 2. Comparison of Al and Ti between clinopyroxenes of olivine basalts and clinopyroxenes of transitional basalts of the Bamoun Plateau

Olivine basalts of Bamoun area [4]	Foumban		Koutaba	
Samples	N8	N13	I4	P2
Al	0,1391 – 0,1756	0,1487 – 0,1769	0,1859 – 0,2478	0,1860 – 0,2347
Ti	0,0709 – 0,07019	0,0708 – 0,0723	0,0771 – 0,0856	0,0772 – 0,0859
Transitional basalts (This study)				
Samples	ZB7	ZB2	ZB55	ZB59
Al	0,066 – 0,100	0,059 – 0,094	0,12 – 0,18	0,063 – 0,106
Ti	0,036 – 0,041	0,022 – 0,039	0,036 – 0,117	0,023 – 0,040

Opaque minerals are primary and secondary. The primary opaque minerals (0.5mm of average diameter) appear in the groundmass or are included in augite and plagioclases, while the secondary opaque minerals are fine grains generally disposed along the planes and fissures in augites. The opaque minerals belong to two solid solutions (Figure 6) of titanomagnetites which are intermediate components of the magnetite-ulvöspinel and ilmenite series.

4.2. Estimations of Thermobarometric Conditions of Clinopyroxenes and Opaque Minerals

The chemical analyses of the samples (major elements) used for the calculation of geothermobarometric conditions are available on request from the corresponding author via his e-mail address.

4.2.1. Clinopyroxenes

The Alt/Ti diagram with respect to Mg* (Figure 7) shows a low variation of the ratio Alt/Ti in the transitional basalts (about 2.50, except for sample ZB55 (1.27 to 5.32)). Since the substitution of Alt/Ti increases with pressure [17], these variations suggest barometric conditions with low variations of crystallization pressure in the transitional basalts. The Al^{VI} diagram with respect to Al^{VI} (Figure 5d) shows that all the clinopyroxenes of the transitional basalts crystallized in relatively constant low pressure conditions. The geobarometer of Purtika [18] confirmed these tendencies with a maximum value of crystallization pressure of 1.8 Kb in these basalts.

The geothermobarometer of Purtika [18], based only on chemical composition of the clinopyroxenes, gives values from 1110°C to 862°C in the transitional basalts.

4.2.2. Opaque Minerals

The magnetite-ilmenite geothermobarometric program of [19] was used to estimate crystallisation temperatures and oxygen fugacities. In this geothermometer, crystallization temperatures varying from 801°C to 1044°C were obtained in the transitional basalts (ZB7 and ZB2) using the formulae of [20] published by [21]. The oxygen fugacities varied from – 10.34 in ZB7 to – 15.43 in ZB2.

The petrographic and mineralogical study reveals that transitional basalts have been set up by gigantic flows occupying large surface, giving an indication on the fluidity of the parental magma and the estimation of the risk if volcanic activity reoccurs. Some of these basalt outcrops under the alkaline ignimbritic deposits in Bangourain, thus characterizing a variety of eruptive dynamisms at the origin of the risks and hazards observed in the region.

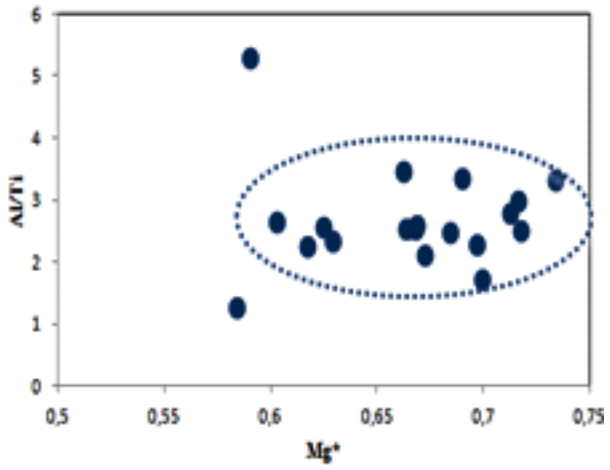

Figure 7. Mg* vs. Al/Ti diagram of the clinopyroxenes. Mg*= Mg/Mg+Fe

4.3. Mapping of the Hazards, Eruptive Dynamisms and Types of Volcanic Risks

To better study the hazards and the risks related to volcanic activities, it was imperative to extend the study area, so as to appropriately evaluate the hazards and risks of the volcanic edifice and the surrounding crater lakes.

4.3.1. Mapping of Volcanic Hazards

The map of Figure 8 shows volcanic hazards in percentages on a graduated scale from 1 to 100 with steps of 10. The hazard map on the west side of the Bamoun plateau is the result of several treatments performed on the satellite images and validated with the field survey. The results obtained were grouped into 5 classes of hazards: (1) from 0 to 20, class of negligible hazards; (2) from 20 to 40, class of low hazards; (3) from 40 to 60, class of mild hazards; (4) from 60 to 80, class of high hazards and (5) from 80 to 100, class of very high hazards.

It is worth noting that, a hazard is the probability for a given region to be affected by a volcanic phenomenon which is potentially destructive for a given time frame, even in a desert milieu [15]. A volcanic risk on the other hand is the mathematic likelihood of the harm caused during a disaster, or it is the probability of a loss (lives, properties, production units) in a region exposed to volcanic risks [27]. The aforementioned results concerning the map of hazards do not take into account human and socio-economic aspects exposed to volcanic threats. The map of hazards was obtained by combining the effect of the following factors: the unit surface with the extension of previous eruptions, the proximity to the volcano, the slope variation in the region and the general topography of the region. This is what explains the accumulation of high and very high hazards around the volcanic cones. A complete study can only be done by associating the following to these results: volcanology studies (different eruptive dynamisms and extension of volcanic products) and demographic data.

4.3.2. Eruptive Dynamisms of Lavas and Types of Volcanic Risks

Several dynamisms have prevailed in the west side of the Bamoun plateau. They include an old effusive volcanism which produced flood basalts, an extrusive volcanism which produced felsic lavas and an explosive episode which produced ignimbrites, ashes, scoria, lapilli, blocks, and bombs. In addition, some evidence of the volcanic activities of the area and the neighboring regions, combined with recent events indicate a possible resumption of activity within them. The evidence include (1) Recent fissure volcanism observed in the prismatic flood of ankaramites at Koutaba and Mamevouo aged 0.82 M years [2]; (2) Recent explosive volcanism in the western Noun plain aged from 2.04 to 1.70 Millions of years, and even more current (0.40 Millions of years) obtained K / Ar whole rocks [28]; (3) Recurrence of landslides in several parts of the sector certainly due to regional microseisms; (4) The recent volcanic activity in the surrounding volcanic regions like Lake Monoun (1984), Lake Nyos (1986), Lake Oku (2011). Field observations then helped to identify the principal risks related to volcanic activities. They are syn-eruptive risks like lava flow, pyroclastic flow, gases and pyroclastic falls, and post-eruptive risks like lahars, lavachas, debris avalanches and blocks.

(1) Syn-eruptive risks

- Pyroclastic flows.

The pyroclastic flows in Bangourain locality are dominated by ignimbrites with a layered aspect (Figure 9a). The extension and the surface area occupied by the ignimbrite confirm the spectacular and dangerous characters of their formation process and the level of disaster that such a phenomenon might cause if it reoccurs. These pyroclastic flows can reach temperatures of about 800°C. Due to the fact that they move at great speed (more than hundreds of Km/h) and can go up hills at times [29], quick warning systems for such phenomena are practically impossible and any attempt to escape is an illusion.

- Lava flows.

Huge basaltic and rhyolitic flows (Figure 9 f, c) are observed in the regions of Nkan'yam and Nkoumelap. The wide extension of the basaltic flow (over 400 m from the eruptive center) testifies their fluid nature during cooling process. Felsic lavas on their part pile up, forming domes in Nkan'yam (Figure 9c). The cooling process of these lavas though spectacular, seems less dangerous for human beings and properties. This is based on the fact that the path of the movement can be known and measures can be taken to deviate the lava flow on time.

- Gases.

The study area is surrounded by two crater lakes which are relatively deep and can contain volcanic gases: lake Nfou on mount Mbépit (at 15 km from Koutaba) and lake Tchoua at Kouoptamo (at 20 km from Nkoumelap), produced by a hydromagmatic or hydro-holomagmatic activity [30]. The case of the neighbouring Monoun maar, where the collapse of the crater wall in the lake triggered the emission of toxic gases of dominating limnologic origin [31] on the night of August 15, 1984 causing the death of 37 people on the west side of the volcano, is an evidence of the dangerous nature of crater lakes in the region. It should be noted that Cameroon is an equatorial country which does not have a very cold season like winter. Therefore the sun maintains an average constant temperature throughout the year making the top layers of

lake water relatively hotter and less dense than the layers beneath. These conditions favour the stratification of limnic water layers containing gases at different densities in the depths of lakes. CO_2 of magmatic origin can then be stocked in the lake's depths for hundreds of years. An external factor like the collapse of a cliff around the crater can provoke the escape of this toxic gas which then becomes disastrous for the surrounding population.

- Pyroclastic fall.

The volcanic projections identified are; blocks, volcanic bombs, lapilli and volcanic ashes (Figure 9 d,e). They are produced from strombolian dynamism in the regions from Tailander to Nkan'yam. The distances between these projections and the eruptive centers (a diameter of about 5km), permit to estimate the probability of the risk. Therefore, the projections of bombs and blocks constitute a risk in the nearer regions while lapilli and ashes are risks in distant regions.

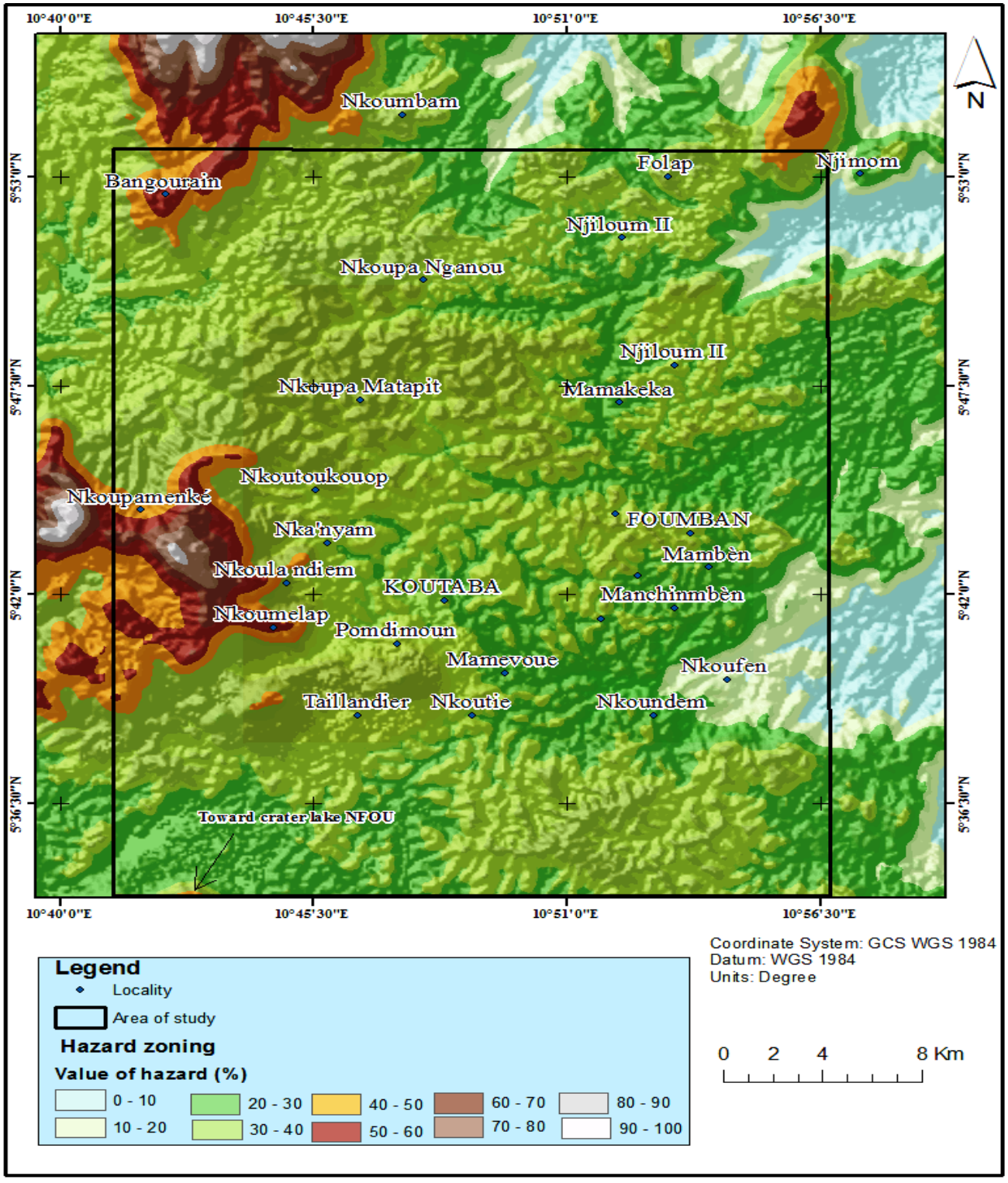

Figure 8. Map of volcanic hazards on the west side of the Bamoun plateau. 0-20: negligible hazards; 20-40: low hazards; 40-60: mild hazards; 60-80: high hazards; 80-100: very high hazards. Combined field and remote sensing applications through the processing of the Landsat-7 Enhance Thematic Mapper Plus (ETM+) were used for the mapping of regional hazard map

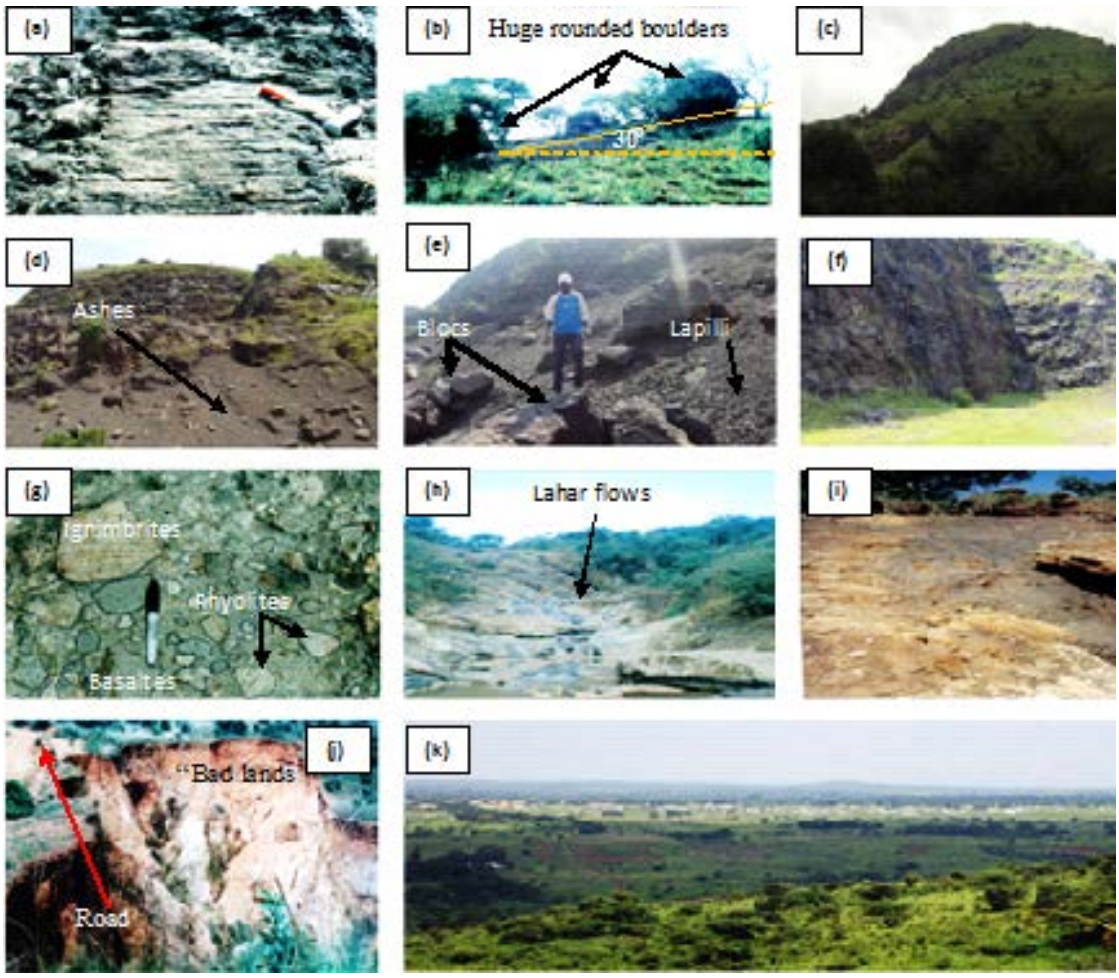

Figure 9. Magmatic formations and associated risks to the west of Bamoun plateau. (a): Ignimbrites with a layered aspect; (b) huge rounded boulders suspended on the slopes of Njitet volcano in Bangourain; (c): feldsic lava dome in Nkan'yam; (d) and (e): volcanic product (ashes, lapilli and blocs) able to be mobilised on the flanks of hills in Nkoumelap. (f) basalt wall in Nkoumelap; (g) rhyolitic matrix of the lahar of Bangourain showing ignimbrite enclaves, basalts and rhyolites; (h) and (i): important extension of lahar of Bangourain respectively by flows in the surrounding valleys and revealed by areolar erosion; (j): "Bad lands" on the road linking the villages of Folap and Bangourain; (k) panoramic view grouping the villages directly exposed to the risks

(2) Post-eruptive risks

- Lahars.

Lahars localised in the Njitet locality in the Bangourain subdivision, are deposits of volcanic materials which are polygenic and heterogenic embedded in a rhyolitic matrix (Figure 9g) and having moved down the steep slopes of hills in the area [32]. They occupy a surface area of about 11.5 km^2 and are concentrated in the valleys and the bed of river Chankié (Figure 9h). The field observations made in the Bangourain area revealed a high degree of weathering from the flanks of the valleys and lahars (Figure 9i). The slopes are thus very abrupt and nearly inaccessible. The weathering process is marked by anthropic activities on the flanks and the regular movement of cattle kept by nomads.

- "Bad lands".

The weathering cover due to huge lava flow is very thick. This phenomenon is the cause of field instability with the formation of ''Bad Lands'' (mazes of narrow ravines and steep ridges over a large area) which dangerously cut across the roads linking some localities (Figure 9j). The ''Bad Lands'' is a hydric erosion which manifests itself when the water, no longer able to infiltrate, runs off and becomes capable of stripping the soil from its upper horizon.

- Debris and block avalanche risks.

The zones threatened by landslides are wildly spread out. These avalanches can be huge and do not follow a given pathway given the volume of rocks and lava blocks suspended on the hill flanks with abrupt slopes (about 30°) (Figure 9b). These blocks mostly have centimetric to decametric sizes and thus can reach high speeds if they happen to collapse, going beyond the valleys along great distances.

4.3.3. The issue

This study is all about the populations and human interests threatened by the phenomena presented. Human lives constitute the most important issue, requiring an imperative estimation of the population directly threatened. Based on the 2006 Cameroon general population census, the hazards' maps proposed and the evaluation of volcanic risks, 1346 families and their properties (settlements and farms) are directly exposed to the different hazards and risks related to volcanic activity. This corresponds to 727/4728 families in Bangourain, 74/273 families in Garap, 101/501 families in Bangambi, 80/285 families in Nkoumelap, 44/932 families in Nka'nyam and 320/8327 families in Nkoupa-Matapit. The threatened population is estimated at 9423 people out of the 53 164 that inhabit the locality, calling for an urgent and strategic proaction!

Nevertheless, today, geotourism and ecotourism, which provide income for guides and the local population, are developed on a local level [33]. Some places, though, are becoming famous like Lake Petponoun, a volcanic dam lake near locality of Foumbot: swimming, boating, golf, volleyball.

5. Conclusion

The west side of the Bamoun plateau presents several petrographic types ranging from feldsic rocks to mafic rocks. Mafic lavas have been identified as basalts without olivine with a transitional character. They are formed in constant conditions of low pressure and relatively high temperatures. The implementation of all lavas and other volcanic products happen by varying eruptive dynamisms inducing a series of hazards and risks that can cause harm to the population and their properties. Significant threats include pyroclastic falls, pyroclastic flows and emission of toxic gases. Mitigation of the volcanic risks is possible, but this requires the combination of different elements among which, the scientific forecasting, the capacity for the authorities to take a decision and the awareness of the population.

Acknowledgements

The authors are grateful to Professor Gilles Chazot (Université de Brest, UMR 6538, Domaines Océaniques, Institut Universitaire Européen de la Mer, France) for the realization of the microprobe analyzes in his laboratory, and the anonymous reviewers for the comments and suggestions that permitted a substantial enhancement of the original manuscript.

References

[1] Moundi, A., Wandji, P., Bardintzeff, J.-M., Ménard, J.-J., Okomo Atouba, L.C., Mouncherou, O.F., Reusser, E., Bellon, H., Tchoua, F.M., 2007. Les basaltes éocènes à affinité transitionnelle du plateau Bamoun, témoins d'un réservoir mantellique enrichi sous la Ligne Volcanique du Cameroun. C.R Géosciences. 339, 396-406.

[2] Moundi, A., Wandji, P., Ghogomu, T.R., Bardintzeff, J.M., Njilah, K.I., Foumboure, I., Ntieche, B., 2009. Existence of Quaternary ankaramites among Tertiary flood basalts at Koutaba (Bamoun Plateau, Western Cameroon): petrology and isotope data. Review of the bulgarian geological society, vol. 70, part 1-3, p. 115-124.

[3] Atouba L.C.O., Chazot G., Moundi A., Agranier A., Bellon H., Nonnotte P., Nzenti J.-P. & Kankeu B., 2016. Mantle sources beneath the Cameroon Volcanic Line: geochemistry and geochronology of the Bamoun plateau mafic rocks. *Arabian Journal of Geosciences*, 9 (4).

[4] Moundi, A., 2004. Les basaltes des plateaux du plateau Bamoun: implication sur les sources des magmas, le contexte et l'évolution géodynamiques. Thèse Doct d'État, Univ. Yaoundé I, 256 p.

[5] Gazel, J., Gerard, G., 1954. Carte géologique de reconnaissance du Cameroun au 1/500000, feuille de Batouri-Est avec notice explicative. Mémoire Direction des Mines et de la Géologie, Yaoundé, Cameroun, 43 p.

[6] Halliday, A.N., Dickin, A., Fallick, A.E., Fitton, J., 1988. Mantle dynamics: a Nd, Sr, Pb and O isotopic study of the Cameroon line volcanic chain. J. Petrol. 29, 181-211.

[7] Burke, K., 2001. Origin of the Cameroon Line of volcano capped-swells. Journal of Geology. 109, 349-362.

[8] Kampunzu, A., Popoff, M., 1991. Distribution of the main Phanerozoic African rifts and associated magmatism: introductory notes, in: A.B kampunzu, R.T Lubala (Eds), Magmatism in Extensional Structural Settings, The Phanerozoic African Plate.

[9] Takodjou Wambo, J.D., Ganno, S., Afahnwie, N.A., Nomo, N.E., Mvondo, O.J., Nzenti, J., 2016. Use of Landsat 7 ETM+ Data for the Geological Structure Interpretation: Case Study of the Ngoura-Colomines Area, Eastern Cameroon. Journal of Geosciences and Geomatics, 4 (3): 61-72.

[10] Leterrier, J., Maury, R., Thonon, P., Girad, D., Marchal, M., 1982. Clinopyroxene composition as a method of identification of the magmatic affinities of paleoseries. Earth and Planetary Science Letters. 59, 139-154.

[11] Lundstrom, C.C., Shaw, H.F., Ryerson, F.J., Williams, Q., Gill, J., 1998. Crystal control of clinopyroxene-melt partitioning in the Di–Ab–An system: implications for elemental fractionations in the depleted mantle. Geochimica et Cosmochimica Acta 62, 2849-2862.

[12] Hill, E., Wood, B.J., Blundy, J.D., 2000. The effect of Ca-Tschermaks component on trace element partitioning between clinopyroxene and silicate melt. Lithos 53, 203–215.

[13] Wood, B.J., Trigila, R., 2001. Experimental determination of aluminous clinopyroxene–melt partition coefficients for potassic liquids, with application to the evolution of the Roman province potassic magmas. Chem. Geol. 172, 213-223.

[14] Gautier, I., Weis, D., Mennessier, J.-P., Vidal, P., Giret, A., Loubet, M., 1990. Petrology and geochemistry of the Kerguelen Archipelago basalts (South Indian Ocean): Evolution of the mantle sources from ridge to intraplate position, Earth Planet, Sci. Lett. 100, 59-76.

[15] Bardintzeff, J.M., 1995. Des risques volcaniques variés: pendant et après l'éruption. Géologues. 106, 19-22.

[16] Guillou, H., Guille, G., Brousse, R., Bardintzeff, J.-M., 1990. Évolution des basaltes tholéiitiques vers des basaltes alcalins dans le substratum volcanique de Fangataufa (Polynésie française), Bull. Soc. geol. France 8 (VI) 3, 537–549.

[17] Boumedhi A., 1988. Les clinopyroxènes dans les basaltes alcalins continentaux (massif central France): Implications pétrogénétiques, barométriques et caractérisation de la profondeur des reservoirs magmatiques. Thèse Doct., Clermond-Ferrand II, 174p.

[18] Putirka, K., 2008. Thermometers and barometers for volcanic systems. In: Putirka, K., Tepley, F. (Eds.), Minerals, Inclusions and Volcanic Processes. Review in Mineralogy and Geochemistry, Miner. Soc. Am. 69, pp. 61-120.

[19] Lepage, L.D., 2003. ILMAT: A Magnetite-Ilmenite Geothermobarometry Program.

[20] Andersen, D.J., Lindsley, D.H., 1988. Internally consistent solution models for Fe-Mg-Mn-Ti oxides; Fe-Ti oxides. American Mineralogist. 73, 714-726.

[21] Nassir, S., 1994. PTOXY: Software package for the calculation of pressure-temperature-oxygen fugacity using a selection of metamorphic geothermobarometers. Computers & Geosciences. 20 (9), 1297-1320.

[22] Morimoto, N., Fabriès, J., Ferguson, A.K., Ginzburt, I.V., Ross, M., Seifert, F.A., Zussman, J., 1988. Nomenclature of pyroxenes. Mineralogy Magmatism. 52, 535-550.

[23] Aoki, K.I., Kushiro, I., 1968. Some clinopyroxenes from ultramafic inclusions in Dreiser weeher, Eifel. Contributions to Mineralogy and Petrology. 18, 326-337.

[24] Aoki, K.I., Shiba, I., 1973. Pyroxenes from lherzolites inclusions of Itinonagata, Japan. Lithos. 6, 41-51.

[25] Caldeira, M., Munhá, J.M., 2002. Petrology of ultramafic nodules from São Tomé Island, Cameroon Volcanic Line (oceanic sector). Journal of African Earth Sciences. 34, 231- 246.

[26] Jagoutz, E., Palme, H., Baddenhaussen, H., Blum, K., Cendales, M., Dreibus, G., Spettel, B., Lorenz, V., Wanke, H., 1979. The abundances of major, minor and trace elements in the earth's mantle as derived from primitive ultramafic nodules. Proceedings of the 10th Lunar Planetery Science Conference, 2031-2050.

[27] Thouret, J., 1993. Gestion des risques naturels et réalités sociales. Soc.Géol. De France. 20p

[28] Wandji, P., Wotchoko, P., Bardintzeff, J.M., Bellon, H., 2010. Late Tertiary and Quaternary alkaline volcanism in the western Noun plain (Cameroon Volcanic Line): new K-Ar ages, petrology and isotope data. Bulgarian Academy of Sciences. 48, 67-94.

[29] Gaudru, H., Pradal, E., 2013. A la découverte des volcans extrêmes. Vuibert, 192 pp.

[30] Wandji, P., Ménard, J.-J., Tchoua, F.M., 1994. L'activité hydromagmatique récente dans la plaine du Noun (Ouest-Cameroun) et les aléas volcaniques associés. C.R Acad. Sci. Paris, t. 319 (série II), 417-422.

[31] Sigurdsson, H., Devine, J., Tchoua, F.M., Presser, T., Pringle, M.K., Evans, W., 1987. Origin of the lethal gas burst from lake Monoun, Cameroon. J. Volcano. Geotherm. Res. 31, 1-16.

[32] Ziem A Bidias L.A., 2007. Importance géologique et environnementale des ‘‘lahars’’ de Bangourain dans le massif du Mbam (Département du Noun, Ouest-Cameroun). Mém. DEA, Univ. Yaoundé I, 59 p.

[33] Bardintzeff, J.M., Wandji, P., Nkouathio, D., Itiga Z., Wotchoko, P., Tchokona Seuwui, D., Kagou Dongmo, A., Temdjim, R., Moundi, A., Chakam Tagheu, P.J., Tsakack, J.P.F., Mouncherou, O.F., Tiabou, F.A., Ntieche, B., Ziem a Bidias, L.A., 2012. The Cameroon Volcanic Line: landscape, natural hazard and human life. Volcandpark, 1st International Congress on Management and Awareness in Protected Volcanic Landscapes, Olot, Spain, 21-25 May.